BOLETIN DE LA SOCIEDAD ESPAÑOLA DE
Cerámica y Vidrio
www.elsevier.es/bsecv

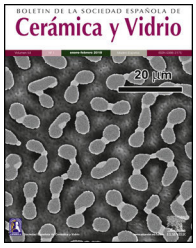

Microwave assisted solution combustion synthesis of β-tricalcium phosphate nano-powders

Davoud Bovand[a,*], *Amir Masoud Arabi*[b], *Maryam Bovand*[c]

[a] *Materials and Metallurgical Engineering Department, Semnan University, Semnan, Iran*
[b] *Department of Inorganic Pigments and Glazes, Institute for Color Science and Technology, Tehran, Iran*
[c] *Department of Biomedical Engineering, Biomaterials Science and Research, Islamic Azad University, Tehran, Iran*

ARTICLE INFO

Article history:
Received 2 October 2017
Accepted 14 May 2018
Available online 1 June 2018

Keywords:
β-Tricalcium phosphate
Combustion method
Fuel
Morphology

ABSTRACT

A new approach for synthesis of β-tricalcium phosphate (β-TCP) was investigated by microwave-assisted combustion method. Three different fuels, glycine, urea and citric acid were used and their effects on the β-TCP powders formation were investigated. The morphology of powders, chemical and phase constituent were determined by SEM, FTIR and XRD, respectively. The results indicated that β-TCP powders with high purity could be obtained when citric acid is used as fuel; and in case of glycine and urea small amounts of hydroxyapatite (HA), calcium pyrophosphate and calcium hydrogen phosphate were detected by XRD. The morphology of β-TCP particles was found to be depended on fuel type. More uniform particle size with higher β-TCP purity was obtained by citric acid as fuel.

Solución de combustión asistida por microondas síntesis de fósforo β-tricálcico Nano-polvos

Palabras clave:
β-Fosfato tricálcico
Método de combustión
Combustible
Morfología

RESUMEN

Se investigó un nuevo método para la síntesis del fosfato β-tricálcico (β-TCP) mediante el método de combustión asistida por microondas. Se utilizaron tres combustibles diferentes, glicina, urea y ácido cítrico, y se investigaron sus efectos sobre la formación de polvos de β-TCP. El componente químico y de fase, la morfología de los polvos fueron determinados por FTIR, XRD y SEM, respectivamente. Los resultados mostraron que se pueden obtener polvos de β-TCP de alta pureza cuando se usa ácido cítrico como combustible, y en el caso de glicina y urea se detectaron pequeñas cantidades de hidroxiapatita (HA), pirofosfato de calcio y fosfato de calcio por XRD. Se encontró que la morfología de las partículas de β-TCP dependía del tipo de combustible. El tamaño de partícula más uniforme con mayor pureza de β-TCP se obtuvo usando ácido cítrico como combustible.

* *Corresponding author.*
E-mail address: davood_bovand@yahoo.com (D. Bovand).
https://doi.org/10.1016/j.bsecv.2018.05.001

Introduction

Calcium phosphate compounds have received much attention for medical science due to the similarity with the inorganic component of bone, satisfactory biocompatibility, bioactivity and osteoconduction characteristics. Among the calcium phosphate compounds, tricalcium phosphate (TCP) with $Ca_3(PO_4)_2$ chemical formula and 1.5 Ca/P ratio is a well-known bio ceramic due to its similarity with the mentioned properties [1–3]. The β-TCP can be used in the human body to repair damaged segments of bones or as bioactive part in orthopedic implants [4].

Hydroxyapatite (HAp: $Ca_{10}(PO4)_6(OH)_2$) is a well-known biomaterial for orthopedic and dental implants and has been extensively investigated since recognized as bioceramic material which possesses proper osteoconduction with chemical composition close to the human skeleton [5].

Tricalcium phosphate has higher resorption and excellent osteoconductivity than HAp and tend to be replaced by bone as degrade. Three different allotropic TCP forms are known as: β-TCP with rhombohedral structure and stability below 1180 °C, α-TCP with monoclinic structure and stability in the temperature range of 1160–1400 °C and α′-TCP with hexagonal structure and stability above 1470 °C. Among different allotropic TCP forms, β-TCP showed accelerated degradation and the most optimal reactivity with the surrounding tissues [6]. The β-TCP powders can be prepared by different techniques such as chemical precipitation, mechanochemical, sol gel, hydrothermal, and solution combustion synthesis (SCS) [7–11]. Factors such as precursors, impurities, crystal size, morphology, PH, type of fuels and heat treatment can affect bioceramics bioactivity.

Solution combustion synthesis starts with nitrates dissolving (e.g., metal nitrates) as oxidant and fuels such as glycine, sucrose, urea, or other water soluble carbohydrates as a reducing reagent. In this method, exothermic reaction occurs in a certain temperature which can be supplied by conventional heating in furnace or under microwave radiations that becomes self-sustaining, resulting a powder as the final product. Calcium phosphate powders can be prepared by calcium nitrate and ammonium phosphate in an aqueous solution with a fuel. Moreover, microwave heating is a more desirable due to the short processing and volumetric heating [12].

Previous studies on synthesis of β-tricalcium phosphate by wet chemical route show that the resultant powder often contains biphasic calcium phosphate phases (i.e., HA and β-tricalcium phosphate) which needs calcination at high temperatures (approximately 950–1200 °C) to transform HA to β-tricalcium phosphate. Published works indicated that changes in the process parameters such as liquid–solid mixture precipitation with fast damping reagents addition, vigorous stirring associated with PH adjustment, Ca/P ratio and/or decreasing in water amount result changes in the constituent phase and products [13,14].

According to the literature few studies investigated the synthesis of pure β-tricalcium phosphate by solution combustion synthesis followed by low temperature calcination (700–1000 °C).

In this study, the effect of different fuel types on β-TCP formation was investigated as well as the formed β-TCP yield.

Experimental procedure

β-Tricalcium phosphate (β-TCP) powder was obtained by microwave assisted solution combustion. $Ca(NO_3)_2{\cdot}4H_2O$ (99% Pure, MERK) and $(NH_4)_2HPO_4$ (99% Pure, MERK) were used as oxidizer and phosphorous source, respectively. Glycine, citric acid and urea (99% Pure, MERK) were used as fuels. Ca/P molar ratio fixed at 1.5 and proper amounts of fuel were calculated according to the stoichiometric equation as follows:

$$3Ca(NO_3)_2 \cdot 4H_2O + 2(NH_4)_2HPO_4 + 2C_2H_5NO_2 \rightarrow Ca_3(PO_4)_2 + 26H_2O + 4CO_2 + 6N_2 \quad (1)$$

$$3Ca(NO_3)_2 \cdot 4H_2O + 2(NH_4)_2HPO_4 + 3CO(NH_2)_2 \rightarrow Ca_3(PO_4)_2 + 27H_2O + 3CO_2 + 8N_2 \quad (2)$$

$$3Ca(NO_3)_2 \cdot 4H_2O + 2(NH_4)_2HPO_4 + C_6H_8O_7 \rightarrow Ca_3(PO_4)_2 + 25H_2O + 6CO_2 + 5N_2 \quad (3)$$

As a typical procedure, stoichiometric mixture of $Ca(NO_3)_2{\cdot}4H_2O$ and mentioned fuels, typically 4.72 g $Ca(NO_3)_2{\cdot}4H_2O$, 1 g glycine,1.20 g urea and 1.28 g citric acid, were dissolved in a 5 ml of deionized water at room temperature in uncovered glass baker, stirred by a magnetic stirrer. In this step, 1.76 g of $(NH_4)_2HPO_4$ was added to the solution under vigorous stirring to form milky suspension. Solution PH was adjusted at 7.5 by adding ammonia solution dropwise (25%). Then, nitric acid was added until the clear solution formation (in this step PH of solution was 1.6) by increasing the temperature to 70 °C. The viscose solution was formed after 10 min. The obtained gel was transferred to microwave oven and irritated for 50 s at 900 W to form spongy-like powder. Final product was procured by mixtures combustion and calcination in an alumina crucible at 850 °C for 2 h in a chamber furnace. They were marked as UR, GL and CA for urea, glycine and citric acid as fuel, respectively. Similarly, samples without the calcination were marked as UR-BC, GL-BC, and CA-BC.

Structural analysis of powders was investigated by X-ray diffraction (XRD, pw1800, PHILIPS company) using Cu Kα radiation ($\lambda = 0.15418$ nm). The average crystallite size was determined by XRD patterns of the peak corresponding to (0 2 10) and Debye–Scherrer's formula as follows:

$$D = \frac{0.9\lambda}{\beta \cos\theta} \quad (4)$$

where D is the crystallite size, λ is the wave length of incident rays, β is full width of the peak at half of maximum (FWHM) and θ is the diffraction angle. Fourier transform infrared (FTIR) (PerkinElmer Company) was used to confirm the sample structure and identifying the functional group. In order to FTIR

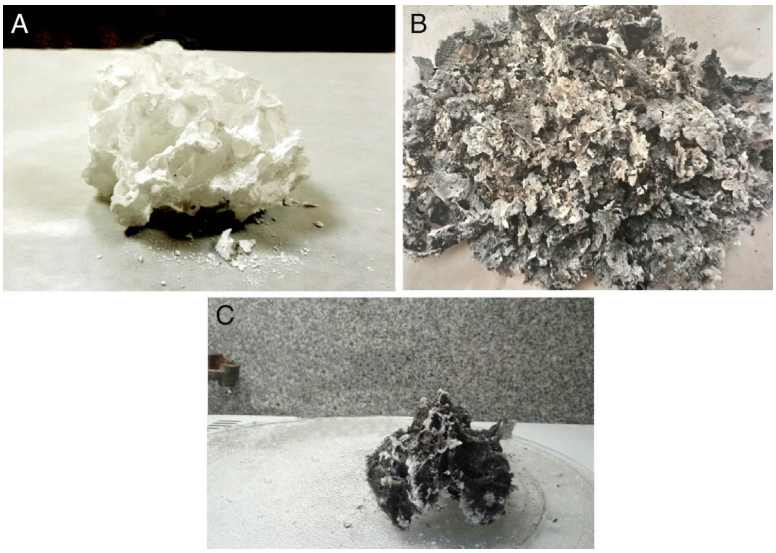

Fig. 1 – Macro-image of voluminous product after combustion with (A) urea, (B) citric acid and (C) glycine.

Table 1 – Relevant thermodynamic data [9,15].

Compound	ΔH_f (kcal/mol)	C_P (cal/mol K)
$Ca(NO_3)_2{\cdot}4H_2O$	−509.37	–
$(NH_4)_2HPO_4$	−374.50	–
$C_2H_5NO_2$	−126.30	–
$CO(NH_2)_2$	−79.71	–
$C_6H_8O_7$	−368.75	–
$Ca_3(PO_4)_2$	−988.2	56.4
O_2	0	7.01
N_2	0	6.8
CO_2	−94.051	11.16
H_2O	−57.796	8.025

analysis the powdered samples dispersed into KBr pellet and spectra was developed over a range of 400–4000 cm^{-1}. Morphology of obtained samples was studied by scanning electron microscopy (SEM, 1455vp, LEO Ltd) equipped with energy dispersive X-ray spectrometer (EDX), the samples were coated with a gold sputter (desk sputter coater II, nano structured coating Co.) before being examined using the SEM.

Results and discussions

Fig. 1 shows the powders after combustion and the color modifies from black to white; base on fuel type. Black color indicates higher residual carbon due to the complete combustion. Citric acid and glycine showed similar combustion with black product whereas for urea the product appeared white.

According to the thermodynamics data from Table 1, and substituting corresponding value in Eqs. (5) and (6) the enthalpy of reaction and adiabatic flame temperature (T_{ad}) of different fuels can be calculated which summarized in Table 2.

$$\Delta H_{combustion} = \left(\sum n\Delta H_f\right)_{products} - \left(\sum n\Delta H_f\right)_{reactant} \quad (5)$$

Table 2 – Effect of fuel type on enthalpy of combustion, adiabatic flame temperature and mole of gases evolved.

Fuel type	Heat of formation ΔH° kcal/mol	Adiabatic flame temperature T_{ad} in K	Volume of exhaust gases (moles)
$C_2H_5NO_2$ (glycine)	−337.23	1260	36
$CO(NH_2)_2$ (urea)	−314.44	1169	38
$C_6H_8O_7$ (citric acid)	−351.39	1279	36

$$\Delta H_{combustion} = \int_{298}^{T_{ad}} \left(\sum nC_p\right)_{products} dT \quad (6)$$

$$T_{ad} = 298 + \frac{(\Delta H_f)_{reactant} - (\Delta H_f)_{product}}{(C_p)_{product}} \quad (7)$$

where n is the number of mole, ΔH_f is standard molar enthalpy (heat) of formation, C_p is heat capacity and T_{ad} is the adiabatic flame temperature which decreases in the citric acid< glycine< urea respect.

Fuel type effect on the different samples structure before and after calcination is illustrated in Fig. 2. As shown in the patterns, CA-BC shows only poor crystalline β-TCP (JCPDS No. 09-0169) phase and GL-BC shows poor crystalline β-TCP and hydroxyapatite (JCPDS No. 09-0432) as a major and minor phase respectively, but the UR-BC structure differs from the others intensely and rather consists of β-TCP as major and CaHPO4 (JCPDS No. 00-003-0423) and $Ca_2P_2O_7$ (JCPDS No. 00-017-0499) as minor phases. Fig. 2 shows that after calcination the peak corresponded to the $Ca_2P_2O_7$ in urea sample became more intense which indicated increasing in crystallinity of $Ca_2P_2O_7$; Moreover the $CaHPo_4$ phase completely disappeared after calcination which can be attributed to the condensation of hydrogenophosphate ions (HPO_4^{2-}) due to the calcium

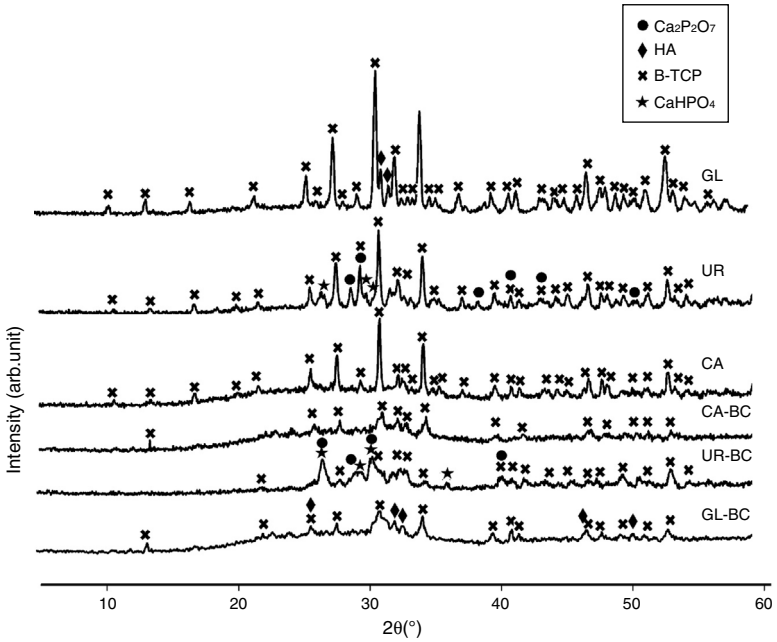

Fig. 2 – XRD patterns of calcium phosphate samples.

Table 3 – Phase constituent of powders obtained with different fuel.

Sample code	Fuel type	Major phase	Minor phase
GL	$C_2H_5NO_2$ (glycine)	β-TCP	$Ca_{10}(PO_4)_6OH_2$ (HA)
UR	$CO(NH_2)_2$ (urea)	β-TCP	$Ca_2P_2O_7$, $CaHPO_4$
CA	$C_6H_8O_7$ (citric acid)	β-TCP	–
GL-BC	$C_2H_5NO_2$ (glycine)	β-TCP	–
UR-BC	$CO(NH_2)_2$ (urea)	β-TCP	$Ca_2P_2O_7$, $CaHPO_4$
CA-BC	$C_6H_8O_7$ (citric acid)	β-TCP	–

deficiency to form pyrophosphates ($P_2O_7^{4-}$) as given in following equation [16].

$$2Ca^{2+} + 2HPO_4^{2-} \rightarrow Ca_2P_2O_7 + H_2O \quad (8)$$

The $Ca_2P_2O_7$ in urea remained stable after calcination. It must be noted that according to the Sha et al. [16], $Ca_2P_2O_7$ transformed to B-TCP at 790 °C which is in contrast to our study. In GL sample, a weak peak related to hydroxyapatite was observed. XRD pattern of CA sample shows no peaks related to calcium pyrophosphate or hydroxyapatite, indicating a high purity of β-TCP. Table 3 shows the phase constituent of different samples which the CA sample shows the highest and purest β-TCP phase.

Average crystallite size of β-TCP determined by Debye–Scherrer's formula was illustrated in Fig. 3. It can be seen that CA sample has the lowest crystallite size (53 nm) whereas UR and GL samples consist of 69 and 138 nm average crystallites size respectively. It seems that the chelating role of citric acid during the combustion reaction retards the reaction rate and leads to the fine crystallites formation [17].

Other important effects of fuel type can be evaluated by FTIR spectra which illustrated in Fig. 4. The γ_2 bending modes at around 3430 and 1640 cm^{-1} are attributed to the absorbed

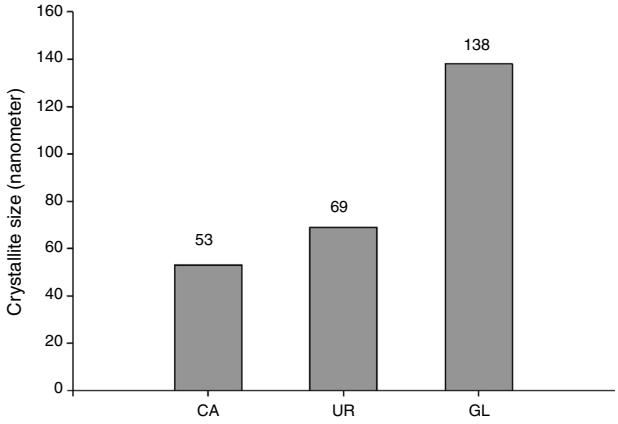

Fig. 3 – Averaged crystallite size of CA, UR and GL samples.

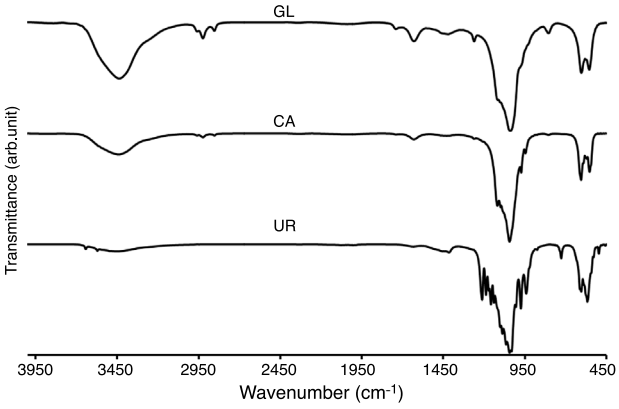

Fig. 4 – FTIR spectra of GL, CA and UR samples.

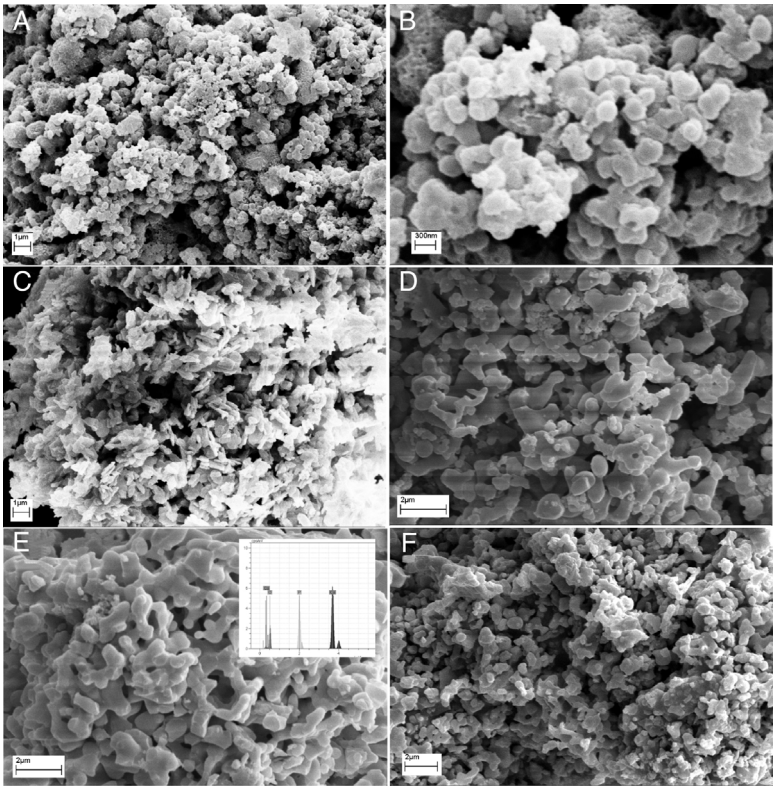

Fig. 5 – SEM image of (A) UR-BC sample, (B) higher magnification of image A, (C) CA-BC sample, (D) GL sample, (E) CA sample and (F) UR sample.

water which was existed in GL and CA samples. The stretching vibrating of hydroxyl groups (OH) of β-TCP powders was observed at around 3000–3600 cm^{-1} which was more intensive for GL sample. The ortho phosphate groups were observed in all samples around 560 and at 1000–1100 cm^{-1} simultaneously, but the narrower peaks of CA sample can be related to the purer structure of ignited sample in the citric acid fuel presence. The peaks at 1210 and 725 cm^{-1} can be assigned to P–O vibrations in pyrophosphate groups in UR sample. The calcium pyrophosphate peaks were not observed in GL and CA samples. It should be noted that calcium pyrophosphate acted as an impurity in β-TCP and deteriorated β-TCP mechanical strength due to the faster resorption of calcium pyrophosphate compared to β-TCP. The CO_3^{2-} group forms weak peaks between 870 and 880 cm^{-1} and more intensive peaks at around 1450 cm^{-1} in GL and UR samples due to the absorption of environment carbon dioxide [12]. The weak bond around 2900 cm^{-1} in GL and CA samples was attributed to the organic contamination during sample preparation with KBr.

Morphological studies of CA, GL and UR samples before and after calcination are illustrated in Fig. 5. It can be clearly seen that the powder size and morphology strongly depend on the fuel type. All samples consist of porous features which may be due to the large volume of exhaust gases during the combustion process, but the size and shape of porosities are highly related to the calcination stage or the fuel type. It seems that both flame temperature and uniform combustion determines the product morphology before calcination. In other words, this difference may be due to non-uniform combustion of powders synthesized by urea compared to citric acid. The BC-CA sample shows two dimensional flake-like morphologies, whereas for urea three dimensional agglomerated regions with spherical primary particles can be distinguished easily. Preparation of flake-like porous microstructure of BC-CA sample can be related to the chelating role of citric acid on the creation of preferred growth in selected planes [17]. Homogenous distribution of semi-spherical particles can be related to the highest temperature of citric acid fuel. Ignition reactions are completed by calcination process and cause the formation of the same homogenous morphologies in CA, UR and GL samples. However, GL consists of coarser and semi-sintered particles. Moreover, localized combustion reaction due to the inhomogeneous gel preparation leads to a specific irregularity in the morphology of BC-UR and UR samples. Other reports indicated a relationship between the amine groups presence of organic fuel and products spongy-like form. It is suggested that glycine fuel decomposes to functional groups of amine in the initial stages of combustion which further decomposes or becomes ignited during the final steps of combustion reaction time or in the calcination process [18].

Fig. 6 shows the SEM of GL sample, As mentioned earlier, in GL sample β-TCP and hydroxyapatite were detected as major and minor phases, respectively. Selected area (Fig. 6B) belongs to the sub 200 nm particles whose EDS analysis is compatible with hydroxyapatite structure. It seems that GL morphologies consist of micro-size semi-sintered particles of β-TCP and up to 200 nm rod-like of hydroxyapatite. Cuneyt Tas [19] reported

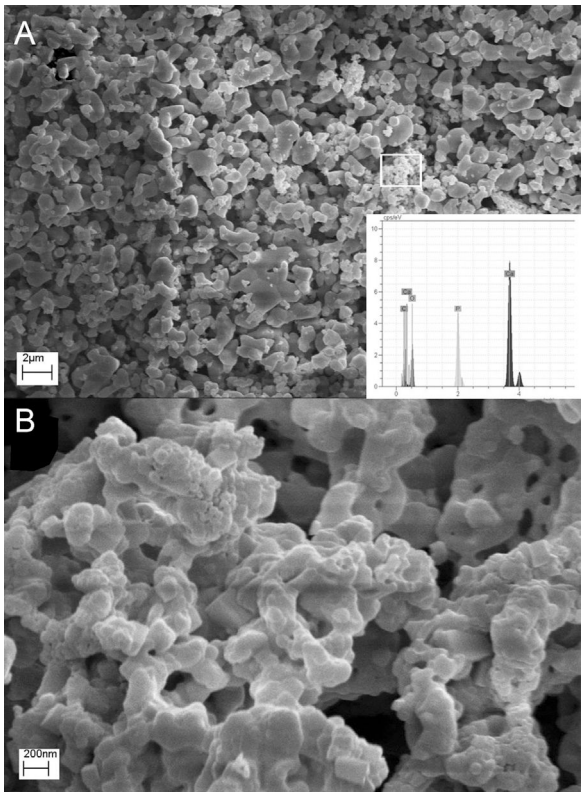

Fig. 6 – SEM image of (A) GL sample with EDS profile of selected area and (B) higher magnification of selected area related to hydroxyapatite phase.

Table 4 – Atomic percentage of GL sample (selected area in Fig. 5) and CA sample.

GL sample		CA sample	
Element	Atomic%	Element	Atomic%
C	4.25	C	0
O	62.77	O	59.42
P	11.63	P	16.39
Ca	21.34	Ca	24.18

the formation of rod-like hydroxyapatite related to high HA stability in solution at PH values higher than 4.2.

The comparison of EDS analysis of GL and CA samples is shown in Table 4. The EDS spectrum shows the presence of Ca, P, O and C. In GL sample, the atomic number percentage of Ca and P for selected area is about 21 and 12, respectively which is close to the hydroxyapatite composition. C presence can be related to unreacted groups of glycine or carbonate absorbed from environment carbon dioxide which was confirmed by FTIR analysis of GL sample. Moreover, EDS analysis of CA sample shows Ca, P and O presence. The atomic percentage of Ca and P is about 24 and 16 respectively, which is in proper agreement with the β-TCP composition. The citric acid is both as chelating agent and fuel. It holds the metal ions together in solution by forming a chelated compound and prevents the precipitation; Moreover ammonia (NH_4OH) increases metal cation chelating with citrates [20]. It can be concluded that the combustion of citric acid fuel due to both ignition and chelating roles leads to the purest composition of β-TCP.

Conclusion

Proper fuel prepared ways to synthesize pure β-tricalcium phosphate powder. Fuel type has effects on phase purity, crystallite size and morphology of products. Pure β-tricalcium phosphate powders were successfully synthesized by microwave assisted solution combustion synthesis with citric acid as fuel. Using urea leads to β-tricalcium phosphate formation as major and calcium pyrophosphate and calcium hydrogen phosphate as minor phases. Urea sample calcination in 850 °C shows transformation of calcium hydrogen phosphate to calcium pyrophosphate. The sample prepared with glycine showed hydroxyapatite as minor phases. The sample synthesized by citric acid showed lower crystallite size with more uniform powder distribution.

REFERENCES

[1] J.K. Chang, et al., Eight-year results of hydroxyapatite-coated hip arthroplasty, J. Arthroplasty 21 (4) (2006) 541–546.
[2] A. Ibara, et al., Osteoconductivity and Biodegradability of Collagen Scaffold Coated with Nano-B-TCP and Fibroblast Growth Factor 2, J. Nanomater. 2013 (2013) 11.
[3] G. Hannink, J.J.C. Arts, Bioresorbability, porosity and mechanical strength of bone substitutes: What is optimal for bone regeneration, Injury 42 (2011) S22–S25.
[4] I. Manjubala, et al., Bioactivity and osseointegration study of calcium phosphate ceramic of different chemical composition, J. Biomed. Mater. Res. 63 (2) (2002) 200–208.
[5] L. Sun, et al., Material fundamentals and clinical performance of plasma-sprayed hydroxyapatite coatings: a review, J. Biomed. Mater. Res. 58 (5) (2001) 570–592.
[6] J. Wiltfang, et al., Degradation characteristics of alpha and beta tri-calcium-phosphate (TCP) in minipigs, J. Biomed. Mater. Res. 63 (2) (2002) 115–121.
[7] S. Lala, B. Satpati, S.K. Pradhan, Sintering behavior and growth mechanism of β-TCP in nanocrystalline hydroxyapatite synthesized by mechanical alloying, Ceram. Int. 42 (11) (2016) 13176–13182.
[8] D. Thomas, et al., Microwave synthesis of functionally graded tricalcium phosphate for osteoconduction, Mater. Today Commun. 9 (2016) 47–53.
[9] T. Volkmer, et al., Novel method for the obtainment of nanostructured calcium phosphate cements: synthesis, mechanical strength and cytotoxicity, Powder Technol. 235 (2013) 599–605.
[10] O. Albayrak, Structural and mechanical characterization of boron doped biphasic calcium phosphate produced by wet chemical method and subsequent thermal treatment, Mater. Charact. 113 (2016) 82–89.
[11] C.M. Mardziah, I. Sopyan, R. Singh, Strontium-doped hydroxyapatite nanopowder via sol-gel method: effect of strontium concentration and calcination temperature on phase behavior, Artif. Organ 23 (2009) 105–113.
[12] N. Bovand, et al., Rapid synthesis of hydroxyapatite nanopowders by a microwave-assisted combustion method, J. Ceram. Process. Res. 13 (3) (2012) 221–225.
[13] J. Liu, et al., The effect of synthetic α-tricalcium phosphate on osteogenic differentiation of rat bone mesenchymal stem cells, Am. J. Transl. Res. 7 (9) (2015) 1588–1601.

[14] M.H. Santos, et al., Synthesis control and characterization of hydroxyapatite prepared by wet precipitation process, Mater. Res. 7 (2004) 625–630.
[15] J. Toniolo, et al., Synthesis of alumina powders by the glycine–nitrate combustion process, Mater. Res. Bull. 40 (2005) 561–571.
[16] L. Sha, et al., Microwave-assisted co-precipitation synthesis of high purity β-tricalcium phosphate crystalline powders, Mater. Chem. Phys. 129 (3) (2011) 1138–1141.
[17] B. Niu, et al., Sol–gel autocombustion synthesis of nanocrystalline high-entropy alloys, Sci. Rep. 7 (1) (2017) 3421.
[18] C.H. Jung, J.Y. Park, W.S. Ryu, Synthesis and dilatometric study of Ca(Sr, La)TiO_3 prepared by solution combustion synthesis (SCS), Solid State Phenom. 119 (2007) 107–110.
[19] A.C. Tas, Combustion synthesis of calcium phosphate bioceramic powders, J. Eur. Ceram. Soc. 20 (2000) 2389–2394.
[20] A. Sutka, G. Mezinskis, Sol–gel auto-combustion synthesis of spinel-type ferrite nanomaterials, Front. Mater. Sci. 6 (2) (2012) 128–141.